



Published in final edited form as:

Cell Rep. 2020 January 21; 30(3): 783–792.e5. doi:10.1016/j.celrep.2019.12.074.

A Mouse Homolog of a Human *TP53* Germline Mutation Reveals a Lipolytic Activity of p53

Ju-Gyeong Kang^{1,7}, Cory U. Lago^{1,7}, Ji-Eun Lee², Ji-Hoon Park¹, Matthew P. Donnelly¹, Matthew F. Starost³, Chengyu Liu⁴, Jaeyul Kwon⁵, Audrey C. Noguchi⁶, Kai Ge², Ping-yuan Wang¹, Paul M. Hwang^{1,8,*}

¹Cardiovascular Branch, National Heart, Lung, and Blood Institute, NIH, Bethesda, MD, USA

²Laboratory of Endocrinology and Receptor Biology, National Institute of Diabetes and Digestive and Kidney Diseases, NIH, Bethesda, MD, USA

³Division of Veterinary Resources, NIH, Bethesda, MD, USA

⁴Transgenic Core, NHLBI, NIH, Bethesda, MD, USA

⁵College of Medicine, Chungnam National University, Daejeon, Korea

⁶NHLBI Murine Phenotyping Core, Bethesda, MD, USA

⁷These authors contributed equally

⁸Lead Contact

SUMMARY

The physiological effects of the many germline mutations of *TP53*, encoding the tumor suppressor protein p53, are poorly understood. Here we report generating a *p53* R178C knockin mouse modeling the human *TP53* R181C mutation, which is notable for its prevalence and prior molecular characterization. Consistent with its weak cancer penetrance in humans, homozygous *p53*^{R178C/C} mice show a modest increase in tumorigenesis but, surprisingly, are lean with decreased body fat content. They display evidence of increased lipolysis and upregulation of fatty acid metabolism in their inguinal white adipose tissue (iWAT). Gene expression and chromatin immunoprecipitation sequencing (ChIP-seq) analyses show that the mutant p53 bound and trans-activated *Beta-3-Adrenergic Receptor* (*ADRB3*), a gene that is known to promote lipolysis and is associated with obesity. This study reveals that a germline mutation of p53 can affect fat metabolism, which has been implicated in cancer development.

This is an open access article under the CC BY-NC-ND license (<http://creativecommons.org/licenses/by-nc-nd/4.0/>).

*Correspondence: hwangp@mail.nih.gov.

AUTHOR CONTRIBUTIONS

J.-G.K., C.U.L., P.-y.W., and P.M.H. conceived and designed the study. J.-G.K., C.U.L., J.-E.L., J.-H.P., M.P.D., M.F.S., C.L., A.C.N., J.K., and P.-y.W. performed the experiments. J.-G.K., C.U.L., J.-E.L., J.-H.P., J.K., K.G., P.-y.W., and P.M.H. analyzed the data. J.-G.K., M.P.D., P.-y.W., and P.M.H. wrote the manuscript.

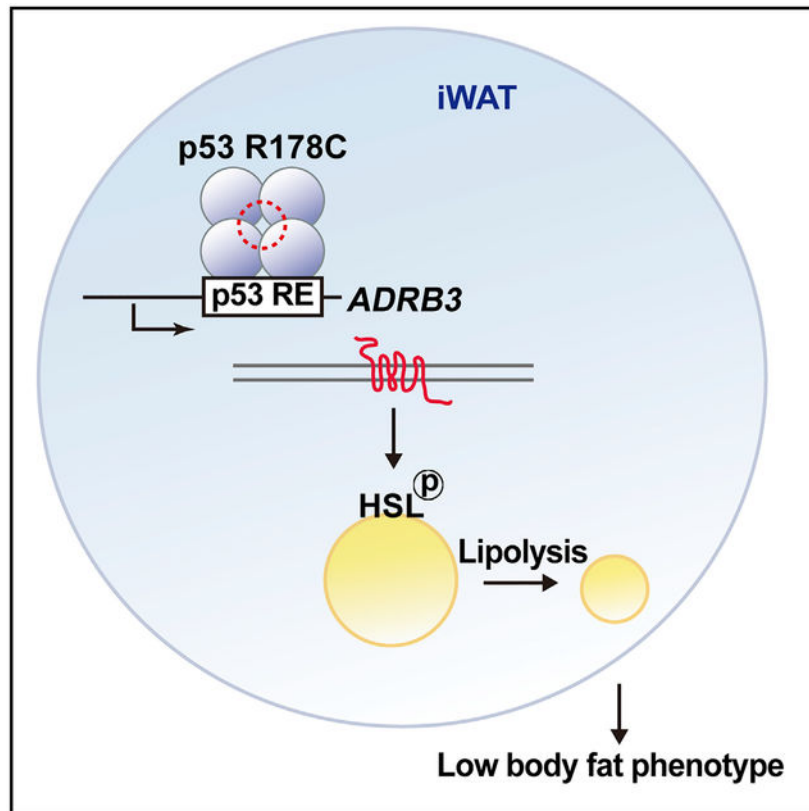
SUPPLEMENTAL INFORMATION

Supplemental Information can be found online at <https://doi.org/10.1016/j.celrep.2019.12.074>.

DECLARATION OF INTERESTS

The authors declare no competing interests.

Graphical Abstract



In Brief

Knockin of the mouse homolog of a human *TP53* germline mutation known to cause Li-Fraumeni syndrome, a cancer predisposition disorder, results in a mouse model characterized by lower body fat content. Kang et al. show that enhancing transactivation of the lipolytic gene *ADRB3* by mutant p53 contributes to this phenotype.

INTRODUCTION

Emerging studies have established p53 as a mediator of various metabolic activities, some of which are sufficient to restrain tumorigenesis even in the absence of its prototypical tumor suppressor functions, such as DNA repair, cell cycle arrest, and apoptosis (Bieging et al., 2014; Kung and Murphy, 2016; Li et al., 2012). p53 can also regulate energy homeostasis through both mitochondrial and non-mitochondrial pathways, including disposition of fatty acids, a major energy substrate and biosynthetic precursor required for cell proliferation (Berkers et al., 2013). Although wild-type p53 inhibits both fatty acid synthesis and lipid accumulation, mutant p53 has been shown to enhance fatty acid synthesis by inhibiting AMP-activated protein kinase (AMPK) (Parrales and Iwakuma, 2016; Zhou et al., 2014). Furthermore, mutant p53 cooperates with sterol regulatory element-binding proteins (SREBPs) to upregulate the mevalonate pathway to promote cancer formation (Freed-Pastor et al., 2012). Thus, alterations in lipid signaling molecules, membrane biosynthesis

precursors, and substrates for fatty acid oxidation caused by mutations in p53 have the potential to support tumorigenesis (Currie et al., 2013). Whether these disparate effects of wild-type and mutant p53 on fatty acid metabolism are generalizable to other germline *TP53* mutations is currently unclear.

Although many different germline mutations of *TP53* have been reported, only a subset of mostly missense mutations located in the DNA binding domain have been associated with Li-Fraumeni syndrome (LFS), an autosomal dominant early-onset cancer disorder (Schneider and Garber, 2010). In a pilot study comprised of subjects with 10 different mutations, including the “hotspot” R273H and weak cancer penetrance R181C amino acid substitutions, LFS patients displayed evidence of increased oxidative metabolism that, upon inhibition, delayed tumorigenesis in a LFS mouse model (Wang et al., 2017, 2013). Given the critical role of p53 in tumor suppression, lessons from examining its metabolic activities at the organismal level in both wild-type and mutant states may provide insights to further understand their physiological and tumorigenic activities.

*TP53*R181C was one of the earliest mutations described in association with breast cancer at a young age, and it currently stands out as one of the top reported germline mutations (Bouaoun et al., 2016; Sidransky et al., 1992). The incidence of this mutation was so high in a specific population studied for inherited breast cancers that it was likened to the *TP53* R337H founder mutation prevalent in southern Brazil (Achatz and Zambetti, 2016; Lolás Hamameh et al., 2017). Amino acid R181 resides in the DNA binding domain of p53 and plays an important structural role by forming intermolecular salt bridges between p53 monomers for cooperative DNA binding (Schlereth et al., 2010). Because p53 R181C promoted mitochondrial biogenesis in human myoblasts (Wang et al., 2013), we investigated whether this specific mutant could have other metabolic effects *in vivo*. Here we report that, in addition to developing a cancer phenotype, mice with knockin of the *TP53* R181C mouse homolog revealed a role for p53 in lipolysis and adipose tissue metabolism under physiologic conditions.

RESULTS

A Mouse Homolog of a LFS Mutation Reveals a Metabolic Phenotype

To examine the effect of human p53 R181C on metabolism, we generated a knockin mouse with an arginine (CGC)-to-cysteine (TGC) mutation at the corresponding amino acid residue 178 of mouse p53 using conventional embryonic stem cell (ESC)-mediated homologous recombination and the Cre-*loxP* strategy (Figures 1A and S1). Correctly targeted ESC clones containing a *p53* C>T (c.541) missense mutation in exon 5 were identified by genomic DNA PCR, and the resulting mouse genotypes were confirmed by *p53* cDNA sequencing, mouse embryonic fibroblast Southern blotting, and tail DNA PCR (Figures 1A and 1B). The homozygous mutant (*p53*^{I78C/C}) mice displayed a modest but significant decrease in median survival time by meeting the animal study endpoint and had a higher incidence of cancer, although the spectrum of cancer types was similar to that of wild-type mice (Figures 1C–1E). Some conventional approaches to induce p53 in *p53*^{I78C/C} mice and examine expression of its target genes and associated cellular activities showed partial retention of wild-type activity, with apoptosis being significantly reduced. This is consistent

with previous reports of greater loss of apoptosis activity compared with cell cycle regulation in cooperative binding mutants (Figure S2; Schlereth et al., 2010; Timofeev et al., 2013). These observations in *p53*^{R178C} mice were also consistent with the relatively low cancer penetrance of the homologous *TP53*^{R181C} mutation in humans.

In the course of these survival studies, *p53*^{R178C} knockin mice showed a pattern of increased body weight. Therefore, we performed metabolic phenotyping focused on male homozygous mutant mice to maximize the mutant p53 effect and to control for gender dimorphism, although female mice also showed increased body weight (Figure 1F and S3A). The energy expenditure and food intake of homozygous *p53*^{178C/C} mice were similar to that of wild-type mice after normalizing for body mass under both room temperature and thermoneutral conditions (Figure S3B). Notably, body composition analysis showed a significant decrease in the fraction of fat tissue in young as well as older *p53*^{178C/C} mice (Figures 1G and S3C). The amount of lean tissue in *p53*^{178C/C} mice accounted for their increased total body weight, but, in addition, there was a trend of increased lean mass percentage in the mutant compared with the wild-type p53 state, which may underlie the observed modest increase in glucose tolerance versus some other possible mechanism (Figures 1G, S3D, and S3E; Kung and Murphy, 2016). The decrease in fat composition of *p53*^{178C/C} mice, without changes in exercise performance, as reported previously for another LFS mouse model (Figure S3F; Wang et al., 2013), appeared to be a gain of function by the *p53* mutation rather than due to loss of wild-type activity because the fat composition of *p53*^{-/-} mice was similar to that of wild-type controls (Figure 1G).

***p53*^{178C/C} Mice Have Decreased Adipose Tissue and Increased Plasma Fatty Acids**

Given the significantly lower body fat composition of *p53*^{178C/C} mice, we investigated further by quantifying the amount of epididymal white adipose tissue (eWAT), inguinal white adipose tissue (iWAT), and brown adipose tissue (BAT) representing visceral, subcutaneous, and thermogenic types of fat, respectively (Figure 2A). The masses of all three adipose tissue types were lower in *p53*^{178C/C} mice, with a more pronounced effect on iWAT, which showed smaller adipocytes compared with *p53* wild-type or null mice (Figure 2B). Given the various contrasting reports of BAT regulation by p53 (Krstic et al., 2018), we examined BAT mitochondria and the thermogenesis phenotype of *p53*^{178C/C} mice but did not observe significant differences, consistent with only a modest decrease in its mass (Figures 2A and S4A–S4C).

We next examined whether the more substantial changes in white adipose tissues were associated with alterations in blood lipid levels. Although the plasma levels of total cholesterol and triglycerides were relatively unchanged in *p53*^{178C/C} mice compared with the wild-type, as also reported for *p53*^{-/-} mice (Guevara et al., 1999), non-esterified fatty acid (NEFA) levels were significantly higher in the mutant p53 knockin mice under *ad libitum* feeding conditions (Figures 2C and 2D). This difference was attenuated by fasting, suggesting activation of lipolysis signaling by mutated p53, manifested only under basal and homeostatic conditions.

Plasma Metabolomic Analysis Reveals Increased Mobilization of Fatty Acids

To obtain a global profile of the changes in lipid metabolism, we performed metabolomic analysis of plasma obtained from 10-week-old $p53^{178R/R}$, $p53^{178C/C}$, and $p53^{-/-}$ male mice under *ad libitum* feeding conditions. A principal-component analysis (PCA) plot showed clustering of the metabolite levels by $p53$ genotype (Figure 3A). About half of the 706 identified compounds were lipid related, and ~20% were significantly changed by $p53$ genotype status (Figure S5A). Of the top 50 compounds whose levels were changed with the greatest statistical significance in the plasma of $p53^{178C/C}$ mice compared with that of $p53$ wild-type or null mice, 39 were lipid related with a pattern of reduced monoacylglycerol and diacylglycerol levels and increased fatty acid derivatives such as acyl carnitines and acyl glycines (Figures 3B and S5B). The increase in acyl carnitines was complemented by a decrease in free carnitine levels (Figure 3C). Interestingly, 12,13-dihydroxy-9Z-octadecenoic acid (12,13-diHOME), a lipokine reported to be induced by cold exposure and inversely correlated with body mass index in human subjects (Lynes et al., 2017), was increased in plasma of $p53^{178C/C}$ mice (Figure 3D). Its precursor linoleic acid and a related compound, 9,10-diHOME, were also increased, providing additional support for the specificity of the 12,13-diHOME lipokine finding (Figure 3D). The elevation of plasma 12,13-diHOME was consistent with the low-fat phenotype of $p53^{178C/C}$ mice and its known promotion of fatty acid utilization in peripheral tissues (Lynes et al., 2017; Stanford et al., 2018).

$p53^{178C/C}$ iWAT Gene Expression Analysis Shows Increased Expression of Lipid Metabolism Genes

The absence of the lipidomic changes in $p53$ -null plasma raised the possibility that a metabolic activity specifically induced by mutant $p53$ may be conferring the low-fat phenotype of $p53^{178C/C}$ mice. Because mutations of $p53$ can affect gene expression of various biological processes, we investigated whether $p53$ R178C can regulate the transcription of genes related to lipolysis (Kasthuber and Lowe, 2017; Pfister and Prives, 2017). We first examined the level of lipolytic activity associated with the $p53$ R178C mutation in different explanted tissues by measuring their glycerol release (Figure 4A). iWAT tissue showed a large increase in lipolytic activity associated with the $p53$ mutation, whereas other adipose tissue types as well as muscle and liver showed no discernable changes (Figure 4A). Therefore, we performed RNA sequencing (RNA-seq) on iWAT tissue in the basal state under which the lipolysis phenotype of $p53^{178C/C}$ mice was observed.

Of all identified genes expressed in iWAT, 528 (~4%) and 1,472 (~12%) were up- and downregulated, respectively, in $p53^{178C/C}$ compared with wild-type mice, using a significance threshold of $p < 0.05$ (Figure 4B). Functional pathway analyses of the RNA-seq data showed upregulation of genes involved in fatty acid metabolism as well as arachidonic acid and cytochrome P450 pathways in the iWAT of $p53^{178C/C}$ mice (Figure 4C). In particular, the upregulation of genes involved in biosynthesis of 12,13-diHOME was in agreement with its elevated plasma levels in $p53^{178C/C}$ mice (Figure S6A). Because the human equivalent of the mouse $p53$ R178 residue mediates DNA binding cooperativity, a mutation at this amino acid would be expected to show reduced $p53$ target gene transactivation, evidenced by decreased expression of the prototypical $p53$ target gene *CDKN1A* (*p21*) (Figure 4D; Schlereth et al., 2010). In contrast, the mRNA expression level

of a key lipolysis enzyme, adipose tissue triglyceride lipase (ATGL), was significantly increased, consistent with the higher lipolytic activity of *p53^{R178C}* iWAT, whereas another important lipolysis enzyme, hormone-sensitive lipase (HSL), and the adipocyte transcription factors PPARG and SREBF were relatively unchanged (Figure 4D). Notably, the expression of β -adrenergic receptor (ADRB3), which is associated with obesity and promotes lipolysis by activating protein kinase A and phosphorylating HSL (Clément et al., 1995; Cypess et al., 2015; Widén et al., 1995; Zechner et al., 2012), was markedly increased in *p53^{R178C}* mouse adipose tissue. These data indicate that the hydrolysis of triglycerides to free fatty acids and their subsequent modification are upregulated by p53 R178C in iWAT.

ChIP-Seq Analysis Identifies *ADRB3* as a p53 Target Gene and Potential Mediator of the *p53^{R178C}* Fat Metabolism Phenotype

To further understand the mechanism underlying the gene expression changes in *p53^{R178C}* mice, we performed chromatin immunoprecipitation followed by sequencing (ChIP-seq) to create a genomic profile of wild-type and mutant p53 binding. Because of the difficulties associated with handling low levels of endogenous p53 in tissues, we utilized a homogeneous primary culture of adipocytes differentiated from the stromal vascular fraction (SVF) of iWAT tissue. Adipocytes differentiated from the *p53^{-/-}* SVF were also utilized for ChIP-seq to screen out non-specific p53 binding peaks. Compared with wild-type cells, immunoblotting of *p53^{R178C}* SVF adipocytes showed higher levels of mutant p53 but lower levels of p21, consistent with its diminished transcriptional activity and increased stabilization, possibly because of loss of its negative feedback regulation (Figure 5A). In contrast to the 6,094 high-confidence (false discovery rate [FDR] < 1E – 10) p53 binding sites identified in wild-type adipocytes by ChIP-seq analysis, only 794 such sites were observed in *p53^{R178C}* adipocytes, the majority (683 sites, 86%) of which were shared with wild-type p53 binding sites (Figure 5B). Because mutated p53 can gain function through association with other transcription factors, we performed a motif search and confirmed that the p53 motif was the most significantly enriched binding sequence for both wild-type and mutant p53 ChIP-seq data (Table S1A; Do et al., 2012; Pfister and Prives, 2017). These analyses indicate that the mutant p53 R178C retains DNA binding specificity, albeit with lower affinity, as suggested previously for other cooperativity mutants of p53 (Schlereth et al., 2010).

Although hotspot mutations of p53 in its DNA binding domain can abolish recognition of p53 binding sequences, we observed a range of binding signals retained by p53 R178C (Figure 5C). Reflecting its partial transactivation of *p21*, p53 R178C binding to the *p21* genomic region appeared to be reduced compared with that of the wild-type protein. It also bound to only one of the two genomic binding sites of *MDM2* compared with wild-type p53, whereas there was complete loss of binding to *BAX* (Figure 5C). Gene Ontology (GO) analysis showed that p53 R178C retains binding to a subset of genomic sites that regulate diverse activities under basal conditions beyond its reported loss of apoptotic activity (Table S1B; Schlereth et al., 2010). Because the increased lipolytic activity of *p53^{R178C}* suggested a “gain of function,” we looked for genes induced by mutant p53 in the iWAT RNA-seq data (>1.2-fold, $p < 0.05$) and integrated them with the p53 R178C ChIP-seq data, resulting in identification of 15 upregulated genes that were bound by mutant p53 (Figure 5D).

Performing a *de novo* motif search on these genes yielded the p53 binding sequence as the only significantly enriched transcription factor motif, confirming a direct interaction with the mutant p53 (Figure 5D). Among these upregulated genes, *ADRB3* stood out as a potential mediator of the adipocyte lipolysis phenotype, possessing a conserved p53 response element (RE) proximal to the 3' region of the gene (Figure 5E).

Interestingly, the *de novo* motif analysis of the 15 p53 R178C upregulated genes revealed that the mutant protein preferentially binds to the p53 RE, with its core (CWWG) flanked by GC-rich sequences (5' PuGG and 3' PyCC), as reported for other cooperative binding mutants of p53 (Figure 5D; Ciribilli et al., 2013; Schlereth et al., 2013). Because the p53 RE of *ADRB3* also showed higher GC content compared with p21, we tested whether it was required for more effective transactivation by the mutant p53 with loss of cooperative binding (Figure 5F). Indeed, a luciferase reporter construct with the *ADRB3* p53 RE flanking sequences mutated from GC to AT showed marked loss of transactivation by both wild-type and mutant p53 protein, indicating their critical importance for p53 interaction with its target gene (Figure 5F). In contrast, increasing the GC content of the p53 RE of *p21* resulted in increased transactivation by p53 R178C to a level comparable with that of wild-type p53, further demonstrating that the flanking GC sequences may obviate the need for cooperative p53 binding to its target genes, as suggested previously (Figure 5F; Jordan et al., 2012).

p53 R178C Regulates ADRB3 and Lipolysis in Adipocytes

Given the direct interaction between mutant p53 and the *ADRB3* gene, we set out to clarify its functional significance. The increased expression of *ADRB3* in the iWAT of *p53^{178C/C}* mice relative to *p53^{178R/R}* and *p53^{-/-}* mice correlated with the levels of basal p53 and phosphorylated HSL, known to be activated by protein kinase A (PKA) in β -adrenergic receptor-stimulated lipolysis (Figures 6A and 6B; Zechner et al., 2012). To confirm that mutant p53 regulates this pathway, SVF cells isolated from *p53^{178C/C}* iWAT were stably transduced with lentiviral shRNA to knock down p53 and then differentiated into adipocytes. Both non-specific (NS) and p53 shRNA-transduced cells showed similar degrees of adipocyte differentiation, as assessed by oil red O cell staining and HSL expression levels (Figures 6C, 6D, and S6B). The depletion of mutant p53 specifically decreased *ADRB3* mRNA and protein levels in association with decreased PKA activity, HSL phosphorylation and release of glycerol (Figures 6C–6E). We controlled for potential shRNA off-target effects by rescuing these changes with re-expression of p53 R178C and further demonstrating that the human homolog p53 R181C can also confer HSL phosphorylation and *ADRB3* mRNA expression activities in *p53^{-/-}* SVF-derived adipocytes (Figures S6C and S6D).

To demonstrate the role of *ADRB3* in mutant p53-induced lipolysis *in vivo*, we pharmacologically modulated *ADRB3* signaling in wild-type and *p53^{178C/C}* mice. Remarkably, the increased levels of PKA activity and phosphorylated HSL associated with the mutant p53 was reduced to wild-type levels by treatment with the *ADRB3* antagonist SR-59230A (Figure 6F). In contrast, the low basal levels of phosphorylated HSL and PKA substrate in wild-type p53 iWAT were increased to *p53^{178C/C}* levels by treatment with the

ADRB3 agonist CL-316243 (Figure 6F). These molecular alterations in the mediators of lipolysis were accompanied by corresponding changes in fat tissue body composition. Daily injections of the antagonist SR-59230A for 5 days reverted the fat tissue phenotype in $p53^{178C/C}$ mice to that of the wild-type, whereas treatment with the agonist CL-316243 reproduced the lower fat composition of the p53 mutant state in wild-type mice (Figure 6G). Taken together, these data demonstrated that p53 R178C-regulated *ADRB3* expression plays an important role in activating the lipolysis signaling pathway of white adipose tissue and in mediating the lower body fat composition of $p53^{178C/C}$ mice.

DISCUSSION

Because physiologic characteristics can be difficult to discern under heterozygous states in humans, we have created a $p53$ R178C knockin mouse to explore its role in metabolism. In our current study, we have demonstrated that this mouse homolog of the human *TP53* R181C LFS mutation can confer a lipolytic activity that likely contributes to its low body fat phenotype. As observed in *TP53* R181C LFS patients, $p53$ R178C knockin mice displayed a mild cancer phenotype, even in the homozygous mutant state, with a longer median survival time than that of hotspot LFS mouse models (Lang et al., 2004; Olive et al., 2004). Nonetheless, $p53^{178C/C}$ mice showed a unique metabolic phenotype of decreased white adipose tissue mass with evidence of increased fatty acid mobilization by lipolysis that has not been observed in $p53^{-/-}$ or other LFS models, such as $p53^{172H/H}$ mice (Park et al., 2009; Wang et al., 2013). Most genome-wide p53 target gene studies have been performed with cancer cell lines under stimulated conditions (Fischer, 2017). Here we examined the adipose tissue and cells relevant to the phenotype under basal conditions to demonstrate that p53 R178C retains the ability to transactivate *ADRB3* and mediate lipolysis.

The mobilization of fatty acid stores by lipolysis observed in $p53^{178C/C}$ mice is notable because another LFS mouse model with the $p53$ R172H knockin mutation has been shown to have increased mitochondrial β -oxidation, suggesting that concerted promotion of oxidative metabolism by p53 occurs through more than one specific gene or pathway (Wang et al., 2013). As suggested previously, germline p53 mutations could be a double-edged sword from an evolutionary perspective (Wang et al., 2012). On one hand, mutant p53 promotion of fatty acid metabolism could improve endurance running or thermogenesis, both of which are beneficial for organismal survival, but in transformed cancer cells, increased mitochondrial activity can contribute to greater malignancy and metastatic potential (LeBleu et al., 2014; Vazquez et al., 2013). Although likely challenging to detect in LFS patient-derived cells, as observed in heterozygous $p53^{178R/C}$ mice, it will be important to determine whether there are also alterations in lipid metabolism in humans (for example, using adipocytes derived from homozygous *TP53* R181C human iPS cells), but the effects of p53 activity on *in vitro* cell differentiation may be difficult to control (Krstic et al., 2018).

The dual nature of p53 regulation of metabolism under normal conditions and in cancer cells is further exemplified by the genes and metabolites identified in this study. Although increased plasma levels of 12,13-diHOME in $p53^{178C/C}$ mice have the potential to improve metabolic health, they can also stimulate proliferation of breast cancer cells (Lynes et al., 2017; Markaverich et al., 2005; Stanford et al., 2018). The increased expression of

arachidonic acid metabolism genes may also promote breast cancer growth through generation of eicosanoids (Figure S6A; Jiang et al., 2005; Mitra et al., 2011). Consistent with the elevated lipolytic activity, bile acid metabolites were the most highly increased compounds identified in $p53^{178C/C}$ plasma and have been reported to mediate tumor metastasis to lymph nodes (Figure S5B; Lee et al., 2019). There are limited data on the physiological effects of germline LFS mutations, but our $p53^{178C/C}$ mouse model reveals an activity of a relatively common LFS mutation that regulates basal metabolism and may also affect cancer development.

STAR★METHODS

LEAD CONTACT AND MATERIALS AVAILABILITY

Further information and requests for reagents may be directed to and will be fulfilled by the Lead Contact, Paul M Hwang (hwangp@mail.nih.gov). Unique reagents generated in this study will be made available under a standard material transfer agreement.

EXPERIMENTAL MODEL AND SUBJECT DETAILS

Mouse models—All mice were maintained and handled in accordance with the NHLBI Animal Care and Use Committee protocol. $p53^{+/-}$ mice (Jackson Laboratory) were of the C57BL6 strain. $p53^{R178C}$ knockin mice were generated using the conventional embryonic stem (ES) cell-mediated homologous recombination method (Lang et al., 2004; Park et al., 2018). Briefly, a gene-targeting construct containing the CGC (Arg) to TGC (Cys) point mutation in exon 5 of $p53$ and neomycin resistance gene flanked by loxP sites was electroporated into the V6.5 mouse ES cell line. G418-resistant colonies were genotyped by PCR, and two correctly targeted ES clones were injected into blastocysts collected from C57BL/6 mice for producing chimeric mice. The chimeras were then bred with wild-type C57BL/6 mice for germline transmission of the mutant allele. After crossing with CMV-*Cre* mice (Jackson Laboratory) to remove the neomycin resistance gene, the knockin mice were backcrossed for 8 generations into the C57BL/6 genetic background. Male mice (9–32 wk old) were used for animal experiments, except for the cancer-free survival studies in which both female (F) and male (M) mice were used (wild-type R/R, 17 F and 13 M; heterozygous R/C, 17 F and 15 M; homozygous C/C, 17 F and 15 M).

Cell culture—Adipose tissue stromal vascular fraction (SVF) was prepared and differentiated as previously described (Ma et al., 2015). Briefly, iWAT was dissected from mice, minced, digested in buffer (123 mM NaCl, 5 mM KCl, 1.3 mM CaCl₂, 5 mM glucose, 100 mM HEPES, and 4% BSA) containing collagenase (1 mg/ml) at 37°C for 45 min, filtered through a 100 m nylon screen, and centrifuged at 150x g for 5 min at room temperature. Cell pellets were washed twice, resuspended, and cultured in DMEM medium containing 10% FBS and 1% penicillin/streptomycin with daily media changes. For adipocyte differentiation, the isolated SVF cells were stimulated with 0.5 mM isobutylmethylxanthine, 125 μM indomethacin, 5 μM dexamethasone, 20 nM insulin, 1 nM T3 and 1 μM rosiglitazone for 48 h and subsequently maintained with 20 nM insulin and 1 nM T3 for 3–4 d, both in complete DMEM medium. Mouse embryonic fibroblasts (MEF)

were prepared from 13.5 d embryos and cultured in DMEM medium supplemented with 10% FBS and 1% penicillin/streptomycin.

p53 null (*p53*^{-/-}) preadipocyte 3T3-L1 cell line was generated using CRISPR-Cas9 technique (Ran et al., 2013). Cells transfected with mouse p53 CRISPR/Cas9 KO plasmid (Santa Cruz, sc-423509) were subjected to serial dilution for isolating single clones and subsequently treated with 5 μ M nutlin-3 (Sigma) for selection. p53 null clones were selected by p53 western blot and confirmed with genomic DNA sequencing.

METHOD DETAILS

Mouse phenotyping studies—For the cancer-free survival study, the mice were euthanized if any external mass exceeded 2 cm in its largest dimension or when the mouse met moribund criteria. Necropsies and histopathologic diagnoses were performed by qualified veterinary pathologists (Division of Veterinary Resources, NIH). To induce p53 *in vivo*, mice were exposed to 5 Gy total body γ -irradiation (TBI) using a Gammacell 40 (K2K 1 \times 8; MDS Nordion) (Chen et al., 2004) or injected with doxorubicin (20 mg/kg, i.p.) 6 or 18 h, respectively, prior to tissue harvest.

Metabolic phenotyping was performed in male mice to control for gender dimorphism and due to resource limitations. Body composition of non-anesthetized mice was measured using the Minispec NMR analyzer (Bruker). Energy expenditure, food intake, and activity under room temperature (22°C) or thermoneutral condition (29.5°C) were measured using the Open Circuit Calorimetry system (CLAMS, Columbus Instruments). For the glucose tolerance test (GTT) and insulin tolerance test (ITT), mice were fasted for 6 h for after which glucose (1.5 mg/g BW) or insulin (0.5 mU/g BW) was administered by i.p. injection and blood glucose levels were measured after injection using a glucometer (AlphaTrak2, Zoetis) over a 120 min period. Treadmill exercise testing was performed as described previously (Park et al., 2009). For thermogenesis testing, mice were individually caged and exposed to 4°C for 5 h during which hourly core body temperatures were measured per rectum using a mouse thermometer probe (THM-100, Indus Instruments).

For ADRB3 pharmacologic studies, iWAT tissue samples were collected from mice 20 min after injection with control saline or CL316243 (1 mg/kg BW, i.p., Sigma-Aldrich), or 1.5 h after SR59230A (3 mg/kg BW, i.p., Sigma-Aldrich). Longer term effect of these agents on body composition was measured 5 d after daily injections of saline, CL316243, or SR59230A at the same doses noted above.

Southern blotting—Mouse embryonic fibroblasts (MEF) genomic DNA was digested with *EcoRI* and analyzed by Southern blotting. The genomic blot was hybridized with ³²P random primed probe (Exon 1 region, Figure S1; Table S2) in UltraHyb solution (Ambion) at 42°C overnight. The blot was washed with 0.3% SSC + 0.1% SDS at 60°C for 1 h followed by 0.1% SSC + 0.1% SDS at room temperature for 1 h and exposed to X-ray film at -80°C.

Histology and tissue biochemistry—Tissues were fixed in 4% formaldehyde, paraffin-embedded, sectioned, and hematoxylin and eosin stained. Differentiated adipocytes were fixed in 4% formaldehyde, stained with Oil Red O solution (American MasterTech) for 20

min, and washed in PBS. The stain was eluted with 100% isopropanol and quantified by measuring A490 nm. iWAT tissue norepinephrine (NE) levels were measured using a noradrenaline ELISA Kit (AVIVA systems biology).

Lipid analysis and metabolomic profiling—Blood from 10 wk old male mice were collected in EDTA tubes and the resulting plasma samples were frozen in liquid nitrogen. Total cholesterol and triglycerides levels were measured by the NCI Pathology/Histology Laboratory (Frederick, MD). Plasma levels of non-esterified fatty acids (NEFA) were measured using a NEFA kit (Wako). Metabolomic profiling was performed by Metabolon (Durham, NC), and the median value-normalized data were analyzed in MetaboAnalyst 3.0.

Lipolysis assay—Freshly isolated tissue or SVF differentiated adipocytes were incubated in DMEM + 1% fatty acid-free BSA for 1 h. Lipolysis rate was determined by measuring the amount of glycerol released into the medium using Free Glycerol Reagent (Sigma) per manufacturer's protocol. Briefly, 5 μ L of culture media were mixed with 200 μ L of glycerol reagent, incubated at room temperature for 15 min, and measured at 550 nm with a plate reader.

Mitochondrial respiratory complex activity assays—Mitochondria were isolated from brown adipose tissue using standard techniques as previously described (Frezza et al., 2007). Respiratory complex I and IV enzymatic activities were measured using blue-native (BN) gel and in-gel assays. The mitochondrial complexes were resolved using a Invitrogen NativePAGE 4%–16% Bis-Tris gel according to the manufacturer's protocol, and the enzymatic activities were visualized by incubating the gel as follows: respiratory complex I—50 mM potassium phosphate (pH 7.0) buffer containing 0.2 mg/ml Nitro Blue Tetrazolium (NBT, Sigma-Aldrich) and 0.1 mg/ml NADH (Sigma-Aldrich); and respiratory complex IV—50 mM sodium phosphate (pH 7.2) buffer containing 0.4 mg/ml diaminobenzidine (DAB, Sigma-Aldrich) and 1 mg/ml cytochrome *c* (Sigma-Aldrich).

Cell cycle and cellular metabolic assays—CD4⁺ T cells were isolated from mouse spleen using CD4 MicroBeads (Miltenyi) according to the manufacturer's protocol. To measure apoptosis, T cells were stimulated with anti-CD3/anti-CD28 antibodies (eBioscience) for 3.5 d, stained with Annexin V (BD Phar-Mingen), and the apoptotic cells were analyzed by flow cytometry (BD LSR II). For the proliferation assay, splenic CD4⁺ T cells were stained with 5 μ M CellTrace Violet reagent (Thermo Fisher Scientific) prior to stimulation with anti-CD3/anti-CD28 and successive generations of live cells were analyzed by flow cytometry. Proliferation was quantified using cell populations that underwent more than 5 divisions normalized to total live cells. Senescence in MEFs was quantified by staining for b-galactosidase activity as previously described (Senescence β -Galactosidase Staining Kit, #9860, Cell Signaling Technology) (Park et al., 2018). Oxygen consumption rate (OCR) and extracellular acidification rate (ECAR) in MEFs were measured by Seahorse XF 24 Analyzer (Agilent) as previously described (Kang et al., 2014).

Antibodies and immunoblotting—Antibodies used in this study were as follows: ADRB3 and GAPDH (Thermo Fisher Scientific); α -tubulin (Sigma-Aldrich); p21 (CDKN1A, Millipore Sigma); PKA α cat (A-2, Santa Cruz Biotechnology); HSL, phospho-

HSL (Ser660), phospho-PKA Substrate (RRXS*/T*) and p53 (1C12) (Cell Signaling Technology); TFAM, Total OXPHOS Rodent Antibody Cocktail and UCP1 (Abcam).

Protein samples were solubilized in cold RIPA buffer supplemented with protease/phosphatase inhibitors (Roche), resolved by Tris-glycine SDS-PAGE, and transferred to Immobilon-P membrane (Millipore) for standard ECL immunoblotting. For p53 immunoblotting in iWAT tissue, endogenous IgG in the tissue lysate was depleted with Dynabeads Protein G (Thermo Fisher Scientific) prior to gel electrophoresis as previously described (Park et al., 2018).

Lentiviruses and cell transduction—Plasmids containing the sequences of non-specific shRNA and mouse p53 shRNA (Open Biosystems, clone # TRCN0000012361) were used to prepare lentivirus according to manufacturer's protocol (Sigma-Aldrich). The p53 R178C and R181C mutations were introduced into mouse or human p53 cDNA, respectively, using QuickChange II site-directed mutagenesis kit (Agilent technologies), and the human p53 R175H cDNA has previously been described (Wang et al., 2017). Mutations were confirmed by sequencing, and the mutant p53 cDNAs were subcloned into pLEX-MCS plasmid (OpenBiosystems) for lentivirus preparation. The lentivirus and polybrene (6 µg/ml) were added to the SVF cells, and the transduced cells were grown for 2 d followed puromycin (2.5 µg/ml) selection. For transient p53 expression, cells were transduced with the p53 cDNA containing lentivirus and grown for 2 d prior to use.

Luciferase reporter assay—The ~1.2 -kb *p21* and *ADRB3* genomic fragments containing the p53 binding site were cloned into the pGL4.10-luciferase vector (Promega) using the In-Fusion Cloning kit (Takara). Mutations were introduced into these constructs using the QuickChange II kit (Agilent technologies) (see Table S2 for primer sequences). Luciferase activity was measured in *p53*^{-/-} 3T3 L1 cells 24 h after cotransfection with wild-type p53, p53 R178C, or empty vector pcDNA and pGL4.74 plasmid containing the TK promoter and Renilla luciferase as a transfection efficiency control (Dual -Luciferase Reporter Assay System, Promega).

Gene expression analysis—Total tissue RNA was purified using QIAzol Lysis Reagent and the RNeasy kit (QIAGEN), and mRNA was isolated using the Dynabead mRNA Purification Kit (Thermo Fisher Scientific). For RT-PCR, cDNA was synthesized using Superscript IV (Thermo Fisher Scientific), and real-time PCR was performed using SYBR green fluorescence on a HT7900 thermal cycler (ABI) as previously described (Patino et al., 2006). The average cycle threshold (Ct) of the respective gene was normalized to housekeeping gene *TIF* (*EIF3F*) (see Table S2 for primer sequences). For RNA-Seq, mRNAs purified from 2 µg of iWAT total RNA were used to synthesize double-stranded cDNAs using the SuperScript Double-Stranded cDNA Synthesis Kit (Thermo Fisher Scientific).

Chromatin immunoprecipitation (ChIP)—ChIP assay was performed as previously described with some modifications (Lee et al., 2017). Briefly, cells were treated with 1.5% formaldehyde to cross-link at room temperature for 10 min, and their nuclei were isolated by incubating in lysis buffer (20 mM Tris pH 8.0, 85 mM KCl, 0.5% NP-40, supplemented with

protease inhibitors) on ice for 10 min followed by centrifugation at 3000x g for 5 min. The nuclear pellet was resuspended in RIPA buffer (10 mM Tris-Cl, pH 7.5, 1mM EDTA, 0.1% SDS, 0.1% sodium deoxycholate, 1% Triton X-100, supplemented with protease inhibitors) and sonicated at 20% amplitude for 15 s, repeated 20 times. The sheared nuclear extracts were immunoprecipitated with anti-p53 (FL393, Santa Cruz #sc-6243) or control rabbit IgG (Santa Cruz #sc-2027) antibodies (pre-bound with Dynabeads Protein A, Thermo Fisher Scientific) at 4°C overnight. Antibody-bound DNA fragments were eluted in 100 µL of elution buffer (1% SDS, 0.1 M NaHCO₃, supplemented with proteinase K to a final concentration of 100 µg/ml) at 65°C for 5 h and purified by QIAquick PCR Purification Kit (QIAGEN).

Sequencing and computational analysis—Sequencing libraries were constructed using NEBNext Ultra II DNA Library Prep Kit for Illumina (NEB). All ChIP-Seq and RNA-Seq samples were sequenced on the Illumina HiSeq 2500. Sequencing reads were aligned to mouse reference genome mm9 using Bowtie 2. To identify p53 binding regions, we used the ‘SICER’ method with a window and gap sizes of 50 bp. To eliminate non-specific binding of p53 antibody, we compared p53 ChIP-Seq data of *p53*^{-/-} cells with that of *p53*^{78R/R} and *p53*^{78C/C} cells, and a FDR of < 1E 10 was used to find high-confidence p53-binding regions. Heatmaps of p53 binding sites were generated with Python 2.7 scripts and graphics package in R with 50 bp resolution. Kyoto Encyclopedia of Genes and Genomes (KEGG) pathway and Gene Ontology (GO) analyses were performed with DAVID Bioinformatics Resources (<https://david.ncifcrf.gov/>; Huang et al., 2009). Motif search (Table S1A) on the ChIP-Seq data was performed by SeqPos motif tool in Galaxy Cistrome as previously described (Lee et al., 2017). Motif search with a limited number of sequences (< 50, Figure 5D) was done with MEME and TOTOM (<http://meme-suite.org/tools/meme>).

QUANTIFICATION AND STATISTICAL ANALYSIS

Unless otherwise specified, data were analyzed using the two-tailed unpaired t test. For data containing more than 2 experimental groups, one-way ANOVA with Tukey’s posttest analysis was performed using GraphPad Prism (v7.02). Principal component analysis, ANOVA analysis, and heatmap clustering of metabolomic data were performed using MetaboAnalyst 3.0 (<https://www.metaboanalyst.ca/>) (Xia et al., 2015).

DATA AND CODE AVAILABILITY

The accession number for the RNA-seq and ChIP-seq datasets reported in this paper is NCBI Gene Expression Omnibus: GSE132715.

Supplementary Material

Refer to Web version on PubMed Central for supplementary material.

ACKNOWLEDGMENTS

We thank Danielle A. Springer, Michele D. Allen (NHLBI Murine Phenotyping Core), Zu-Xi Yu (NHLBI Pathology Core), William M. Kamp, Somin Kwon, Ryoan Hwan Kim, Deborah Simon, Komudi Singh, and Haiming Cao for helpful advice and assistance during the course of this study. This work was supported by the

National Heart, Lung, and Blood Institute Division of Intramural Research (HL005101-14 to P.M.H.). J.K. was supported by research funding from Chungnam National University, South Korea.

REFERENCES

- Achatz MI, and Zambetti GP (2016). The Inherited p53 Mutation in the Brazilian Population. *Cold Spring Harb. Perspect. Med* 6, a026195. [PubMed: 27663983]
- Berkers CR, Maddocks OD, Cheung EC, Mor I, and Vousden KH (2013). Metabolic regulation by p53 family members. *Cell Metab.* 18, 617–633. [PubMed: 23954639]
- Bieging KT, Mello SS, and Attardi LD (2014). Unravelling mechanisms of p53-mediated tumour suppression. *Nat. Rev. Cancer* 14, 359–370. [PubMed: 24739573]
- Bouaoun L, Sonkin D, Ardin M, Hollstein M, Byrnes G, Zavadil J, and Olivier M (2016). TP53 Variations in Human Cancers: New Lessons from the IARC TP53 Database and Genomics Data. *Hum. Mutat* 37, 865–876. [PubMed: 27328919]
- Chen J, Lipovsky K, Ellison FM, Calado RT, and Young NS (2004). Bystander destruction of hematopoietic progenitor and stem cells in a mouse model of infusion-induced bone marrow failure. *Blood* 104, 1671–1678. [PubMed: 15166031]
- Ciribilli Y, Monti P, Bisio A, Nguyen HT, Ethayathulla AS, Ramos A, Foggetti G, Menichini P, Menendez D, Resnick MA, et al. (2013). Transactivation specificity is conserved among p53 family proteins and depends on a response element sequence code. *Nucleic Acids Res.* 41, 8637–8653. [PubMed: 23892287]
- Clément K, Vaisse C, Manning BS, Basdevant A, Guy-Grand B, Ruiz J, Silver KD, Shuldiner AR, Froguel P, and Strosberg AD (1995). Genetic variation in the beta 3-adrenergic receptor and an increased capacity to gain weight in patients with morbid obesity. *N. Engl. J. Med* 333, 352–354. [PubMed: 7609752]
- Currie E, Schulze A, Zechner R, Walther TC, and Farese RV Jr. (2013). Cellular fatty acid metabolism and cancer. *Cell Metab.* 18, 153–161. [PubMed: 23791484]
- Cypess AM, Weiner LS, Roberts-Toler C, Franquet Elía E, Kessler SH, Kahn PA, English J, Chatman K, Trauger SA, Doria A, and Kolodny GM (2015). Activation of human brown adipose tissue by a b3-adrenergic receptor agonist. *Cell Metab.* 21, 33–38. [PubMed: 25565203]
- Do PM, Varanasi L, Fan S, Li C, Kubacka I, Newman V, Chauhan K, Daniels SR, Bocchetta M, Garrett MR, et al. (2012). Mutant p53 cooperates with ETS2 to promote etoposide resistance. *Genes Dev.* 26, 830–845. [PubMed: 22508727]
- Fischer M (2017). Census and evaluation of p53 target genes. *Oncogene* 36, 3943–3956. [PubMed: 28288132]
- Freed-Pastor WA, Mizuno H, Zhao X, Langerød A, Moon SH, Rodriguez-Barrueco R, Barsotti A, Chicas A, Li W, Polotskaia A, et al. (2012). Mutant p53 disrupts mammary tissue architecture via the mevalonate pathway. *Cell* 148, 244–258. [PubMed: 22265415]
- Frezza C, Cipolat S, and Scorrano L (2007). Organelle isolation: functional mitochondria from mouse liver, muscle and cultured fibroblasts. *Nat. Protoc* 2, 287–295. [PubMed: 17406588]
- Guevara NV, Kim HS, Antonova EI, and Chan L (1999). The absence of p53 accelerates atherosclerosis by increasing cell proliferation in vivo. *Nat. Med* 5, 335–339. [PubMed: 10086392]
- Huang W, Sherman BT, and Lempicki RA (2009). Bioinformatics enrichment tools: paths toward the comprehensive functional analysis of large gene lists. *Nucleic Acids Res.* 37, 1–13. [PubMed: 19033363]
- Jiang JG, Chen CL, Card JW, Yang S, Chen JX, Fu XN, Ning YG, Xiao X, Zeldin DC, and Wang DW (2005). Cytochrome P450 2J2 promotes the neoplastic phenotype of carcinoma cells and is up-regulated in human tumors. *Cancer Res.* 65, 4707–4715. [PubMed: 15930289]
- Jordan JJ, Menendez D, Sharav J, Beno I, Rosenthal K, Resnick MA, and Haran TE (2012). Low-level p53 expression changes transactivation rules and reveals superactivating sequences. *Proc. Natl. Acad. Sci. USA* 109, 14387–14392. [PubMed: 22908277]
- Kang JG, Wang PY, and Hwang PM (2014). Cell-based measurements of mitochondrial function in human subjects. *Methods Enzymol.* 542, 209–221. [PubMed: 24862268]

- Kasthuber ER, and Lowe SW (2017). Putting p53 in Context. *Cell* 170, 1062–1078. [PubMed: 28886379]
- Krstic J, Reinisch I, Schupp M, Schulz TJ, and Prokesch A (2018). p53 Functions in Adipose Tissue Metabolism and Homeostasis. *Int. J. Mol. Sci* 19, E2622. [PubMed: 30181511]
- Kung CP, and Murphy ME (2016). The role of the p53 tumor suppressor in metabolism and diabetes. *J. Endocrinol* 231, R61–R75. [PubMed: 27613337]
- Lang GA, Iwakuma T, Suh YA, Liu G, Rao VA, Parant JM, Valentin-Vega YA, Terzian T, Caldwell LC, Strong LC, et al. (2004). Gain of function of a p53 hot spot mutation in a mouse model of Li-Fraumeni syndrome. *Cell* 119, 861–872. [PubMed: 15607981]
- LeBleu VS, O'Connell JT, Gonzalez Herrera KN, Wikman H, Pantel K, Haigis MC, de Carvalho FM, Damascena A, Domingos Chinen LT, Rocha RM, et al. (2014). PGC-1 α mediates mitochondrial biogenesis and oxidative phosphorylation in cancer cells to promote metastasis. *Nat. Cell Biol* 16, 992–1003, 1–15. [PubMed: 25241037]
- Lee JE, Park YK, Park S, Jang Y, Waring N, Dey A, Ozato K, Lai B, Peng W, and Ge K (2017). Brd4 binds to active enhancers to control cell identity gene induction in adipogenesis and myogenesis. *Nat. Commun* 8, 2217. [PubMed: 29263365]
- Lee CK, Jeong SH, Jang C, Bae H, Kim YH, Park I, Kim SK, and Koh GY (2019). Tumor metastasis to lymph nodes requires YAP-dependent metabolic adaptation. *Science* 363, 644–649. [PubMed: 30733421]
- Li T, Kon N, Jiang L, Tan M, Ludwig T, Zhao Y, Baer R, and Gu W (2012). Tumor suppression in the absence of p53-mediated cell-cycle arrest, apoptosis, and senescence. *Cell* 149, 1269–1283. [PubMed: 22682249]
- Lolas Hamameh S, Renbaum P, Kamal L, Dweik D, Salahat M, Jaraysa T, Abu Rayyan A, Casadei S, Mandell JB, Gulsuner S, et al. (2017). Genomic analysis of inherited breast cancer among Palestinian women: Genetic heterogeneity and a founder mutation in TP53. *Int. J. Cancer* 141, 750–756. [PubMed: 28486781]
- Lynes MD, Leiria LO, Lundh M, Bartelt A, Shamsi F, Huang TL, Takahashi H, Hirshman MF, Schlein C, Lee A, et al. (2017). The cold-induced lipokine 12,13-diHOME promotes fatty acid transport into brown adipose tissue. *Nat. Med* 23, 631–637. [PubMed: 28346411]
- Ma X, Xu L, Alberobello AT, Gavrilova O, Bagattin A, Skarulis M, Liu J, Finkel T, and Mueller E (2015). Celastrol Protects against Obesity and Metabolic Dysfunction through Activation of a HSF1-PGC1 α Transcriptional Axis. *Cell Metab.* 22, 695–708. [PubMed: 26344102]
- Markaverich BM, Crowley JR, Alejandro MA, Shoulars K, Casajuna N, Mani S, Reyna A, and Sharp J (2005). Leukotoxin diols from ground corn cob bedding disrupt estrous cyclicity in rats and stimulate MCF-7 breast cancer cell proliferation. *Environ. Health Perspect* 113, 1698–1704. [PubMed: 16330350]
- Mitra R, Guo Z, Milani M, Mesaros C, Rodriguez M, Nguyen J, Luo X, Clarke D, Lamba J, Schuetz E, et al. (2011). CYP3A4 mediates growth of estrogen receptor-positive breast cancer cells in part by inducing nuclear translocation of phospho-Stat3 through biosynthesis of (\pm)-14,15-epoxyeicosatrienoic acid (EET). *J. Biol. Chem* 286, 17543–17559. [PubMed: 21402692]
- Olive KP, Tuveson DA, Ruhe ZC, Yin B, Willis NA, Bronson RT, Crowley D, and Jacks T (2004). Mutant p53 gain of function in two mouse models of Li-Fraumeni syndrome. *Cell* 119, 847–860. [PubMed: 15607980]
- Park JY, Wang PY, Matsumoto T, Sung HJ, Ma W, Choi JW, Anderson SA, Leary SC, Balaban RS, Kang JG, et al. (2009). p53 improves aerobic exercise capacity and augments skeletal muscle mitochondrial DNA content. *Circ. Res* 105, 705–712, 11 p following 712. [PubMed: 19696408]
- Park JH, Li J, Starost MF, Liu C, Zhuang J, Chen J, Achatz MI, Kang JG, Wang PY, Savage SA, and Hwang PM (2018). Mouse Homolog of the Human TP53 R337H Mutation Reveals Its Role in Tumorigenesis. *Cancer Res.* 78, 5375–5383. [PubMed: 30042151]
- Parrales A, and Iwakuma T (2016). p53 as a Regulator of Lipid Metabolism in Cancer. *Int. J. Mol. Sci* 17, E2074. [PubMed: 27973397]
- Patino WD, Kang JG, Matoba S, Mian OY, Gochuico BR, and Hwang PM (2006). Atherosclerotic plaque macrophage transcriptional regulators are expressed in blood and modulated by tristetraprolin. *Circ. Res* 98, 1282–1289. [PubMed: 16614304]

- Pfister NT, and Prives C (2017). Transcriptional Regulation by Wild-Type and Cancer-Related Mutant Forms of p53. *Cold Spring Harb. Perspect. Med* 7, a026054.
- Ran FA, Hsu PD, Wright J, Agarwala V, Scott DA, and Zhang F (2013). Genome engineering using the CRISPR-Cas9 system. *Nat. Protoc* 8, 2281–2308. [PubMed: 24157548]
- Schlereth K, Beinoraviciute-Kellner R, Zeitlinger MK, Bretz AC, Sauer M, Charles JP, Vogiatzi F, Leich E, Samans B, Eilers M, et al. (2010). DNA binding cooperativity of p53 modulates the decision between cell-cycle arrest and apoptosis. *Mol. Cell* 38, 356–368. [PubMed: 20471942]
- Schlereth K, Heyl C, Krampitz AM, Mernberger M, Finkernagel F, Scharfe M, Jarek M, Leich E, Rosenwald A, and Stiewe T (2013). Characterization of the p53 cistrome–DNA binding cooperativity dissects p53’s tumor suppressor functions. *PLoS Genet.* 9, e1003726. [PubMed: 23966881]
- Schneider K, and Garber J (2010). Li-Fraumeni Syndrome In *GeneReviews*, Pagon RA, et al., (University of Washington). <https://www.ncbi.nlm.nih.gov/books/NBK1311/>.
- Sidransky D, Tokino T, Helzlsouer K, Zehnbauser B, Rausch G, Shelton B, Prestigiacomo L, Vogelstein B, and Davidson N (1992). Inherited p53 gene mutations in breast cancer. *Cancer Res.* 52, 2984–2986. [PubMed: 1581912]
- Stanford KI, Lynes MD, Takahashi H, Baer LA, Arts PJ, May FJ, Lehnig AC, Middelbeek RJW, Richard JJ, So K, et al. (2018). 12,13-di- HOME: An Exercise-Induced Lipokine that Increases Skeletal Muscle Fatty Acid Uptake. *Cell Metab* 27, 1111–1120.e3. [PubMed: 29719226]
- Timofeev O, Schlereth K, Wanzel M, Braun A, Nieswandt B, Pagenstecher A, Rosenwald A, Elsässer HP, and Stiewe T (2013). p53 DNA binding cooperativity is essential for apoptosis and tumor suppression in vivo. *Cell Rep.* 3, 1512–1525. [PubMed: 23665223]
- Vazquez F, Lim JH, Chim H, Bhalla K, Girnun G, Pierce K, Clish CB, Granter SR, Widlund HR, Spiegelman BM, and Puigserver P (2013). PGC1 α expression defines a subset of human melanoma tumors with increased mitochondrial capacity and resistance to oxidative stress. *Cancer Cell* 23, 287–301. [PubMed: 23416000]
- Wang PY, Zhuang J, and Hwang PM (2012). p53: exercise capacity and metabolism. *Curr. Opin. Oncol* 24, 76–82. [PubMed: 22123233]
- Wang PY, Ma W, Park JY, Celi FS, Arena R, Choi JW, Ali QA, Tripodi DJ, Zhuang J, Lago CU, et al. (2013). Increased oxidative metabolism in the Li-Fraumeni syndrome. *N. Engl. J. Med* 368, 1027–1032. [PubMed: 23484829]
- Wang PY, Li J, Walcott FL, Kang JG, Starost MF, Talagala SL, Zhuang J, Park JH, Huffstutler RD, Bryla CM, et al. (2017). Inhibiting mitochondrial respiration prevents cancer in a mouse model of Li-Fraumeni syndrome. *J. Clin. Invest* 127, 132–136. [PubMed: 27869650]
- Widén E, Lehto M, Kanninen T, Walston J, Shuldiner AR, and Groop LC (1995). Association of a polymorphism in the beta 3-adrenergic-receptor gene with features of the insulin resistance syndrome in Finns. *N. Engl. J. Med* 333, 348–351. [PubMed: 7609751]
- Xia J, Sinelnikov IV, Han B, and Wishart DS (2015). *MetaboAnalyst 3.0*—making metabolomics more meaningful. *Nucleic Acids Res* 43, W251–257. [PubMed: 25897128]
- Zechner R, Zimmermann R, Eichmann TO, Kohlwein SD, Haemmerle G, Lass A, and Madeo F (2012). FAT SIGNALS—lipases and lipolysis in lipid metabolism and signaling. *Cell Metab.* 15, 279–291. [PubMed: 22405066]
- Zhou G, Wang J, Zhao M, Xie TX, Tanaka N, Sano D, Patel AA, Ward AM, Sandulache VC, Jasser SA, et al. (2014). Gain-of-function mutant p53 promotes cell growth and cancer cell metabolism via inhibition of AMPK activation. *Mol. Cell* 54, 960–974. [PubMed: 24857548]

Highlights

- Mouse homolog of a *TP53* germline mutation reveals a metabolic phenotype
- Mutant p53 R178C differentially retains wild-type p53 activity
- ChIP-seq analysis identifies adrenergic receptor *ADRB3* as a p53 target gene
- p53 R178C promotes lipolysis in adipocytes by increased ADRB3 signaling

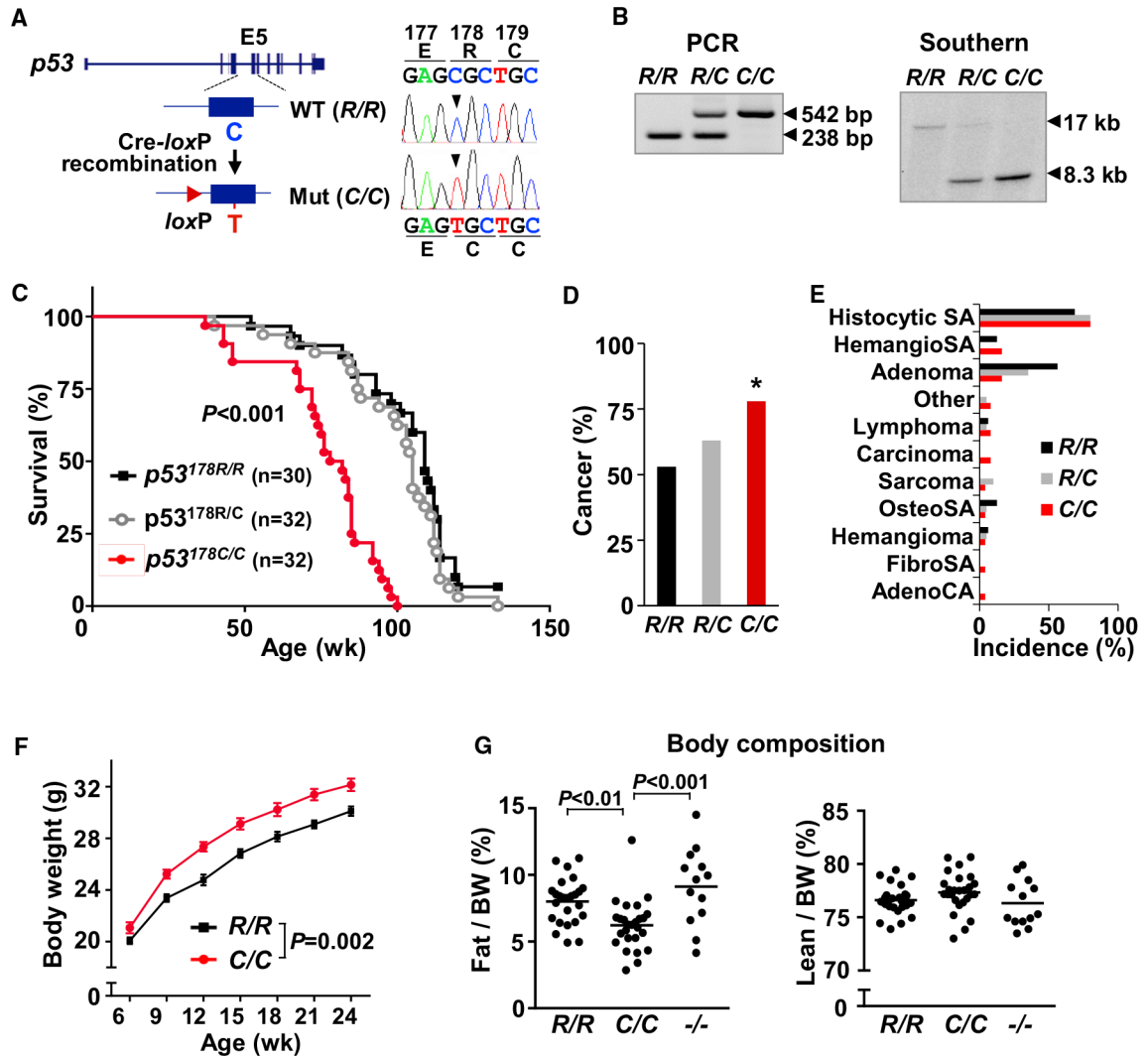


Figure 1. *p53* R178C Knockin Mice Reveal Increased Cancer Incidence and a Metabolic Phenotype
 (A) *Cre-loxP*-mediated strategy for knockin of the amino acid R178C mutation into exon 5 (E5) of the mouse *p53* gene. Mouse embryonic fibroblast (MEF) cDNA sequencing confirmed single-nucleotide substitution from C to T (right panel).
 (B) Genomic DNA samples isolated from tail tissue and MEFs were analyzed by PCR and Southern blot, respectively. The 238-bp and 17-kb fragments correspond to the wild-type *p53* allele. The 542-bp and 8.3-kb fragments correspond to the mutant *p53* allele.
 (C) Kaplan-Meier survival plot of the indicated *p53* genotype mice. Median survival ages (weeks) were as follows: *R/R*, 109; *R/C*, 105; *C/C*, 80. Significance testing in comparison with wild-type *p53*.
 (D) Cancer incidence in mice (*R/R*, n = 30; *R/C*, n = 32; *C/C*, n = 32).
 (E) Spectrum of cancer types by *p53* genotype (*R/R*, n = 16; *R/C*, n = 20; *C/C*, n = 25).
 (F) Body weight of male mice by age (n = 15).
 (G) Fat and lean (muscle) body composition of 9-week-old male mice, measured by NMR analyzer (*R/R*, n = 25; *C/C*, n = 26; *-/-*, n = 13).

p53 R178 genotypes: wild-type *p53*^{178R/R} (*R/R*), heterozygous mutant *p53*^{178R/C} (*R/C*), homozygous mutant *p53*^{178C/C} (*C/C*), and null *p53*^{-/-} (*-/-*). Statistical difference by χ^2 test in comparison with the wild-type (D), two-way ANOVA with repeated measures (F), and one-way ANOVA (G). Values are mean \pm SEM. **p* < 0.05. See also Figures S1–S3.

Author Manuscript

Author Manuscript

Author Manuscript

Author Manuscript

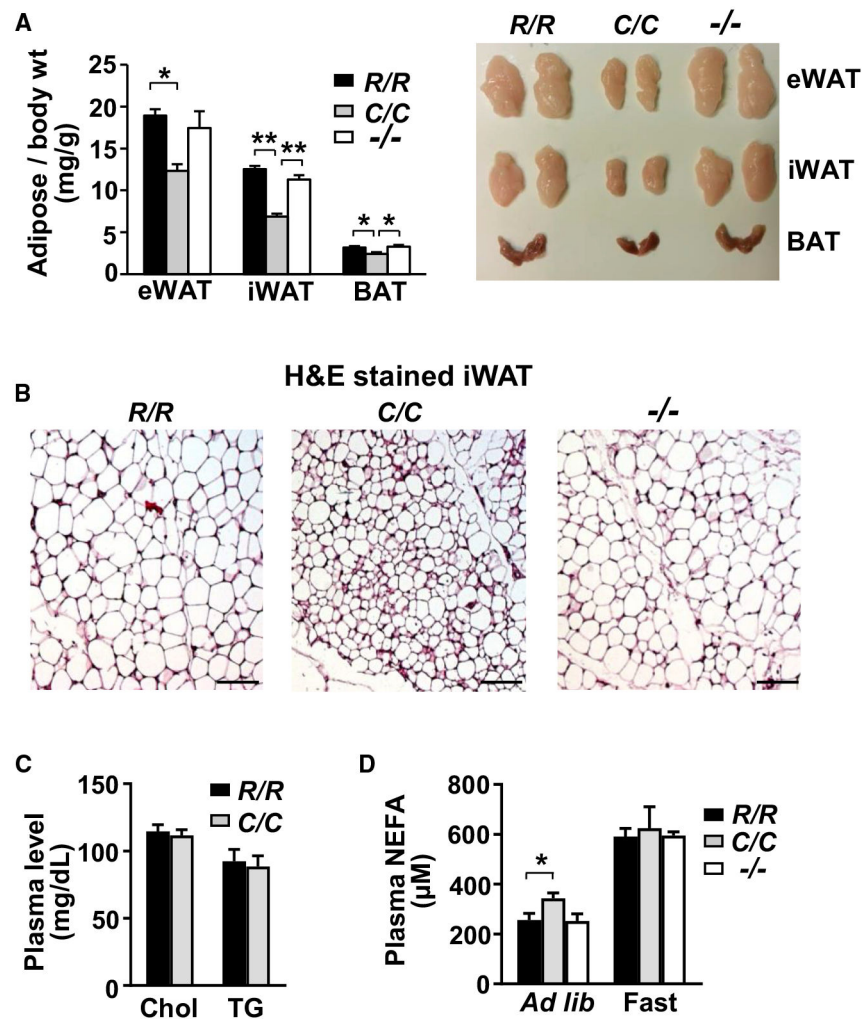


Figure 2. Homozygous $p53^{178C/C}$ Mice Display a Lean Phenotype with Increased Plasma Fatty Acids

(A) Representative images of 3 different fat tissue types: inguinal white adipose tissue (iWAT), epididymal white adipose tissue (eWAT), and brown adipose tissue (BAT). The weight of fat tissue dissected from 10-week-old mice was normalized to body weight (milligrams per gram) ($n = 6$).

(B) H&E-stained iWAT sections. Scale bars, 100 μm .

(C) Plasma lipid levels: total cholesterol (Chol) and triglycerides (TG) ($n = 10$).

(D) Plasma non-esterified fatty acid (NEFA) levels measured under free feeding (*ad libitum*, R/R , $n = 15$; C/C , $n = 23$; $-/-$, $n = 9$) or fasting (fast for 4 h, R/R , $n = 8$; C/C , $n = 11$; $-/-$, $n = 3$) states.

$p53^{R178}$ genotypes: wild-type (R/R), homozygous mutant (C/C), and null ($-/-$). Statistical difference by one-way ANOVA. Values are mean \pm SEM. * $p < 0.05$, ** $p < 0.01$. See also Figure S4.

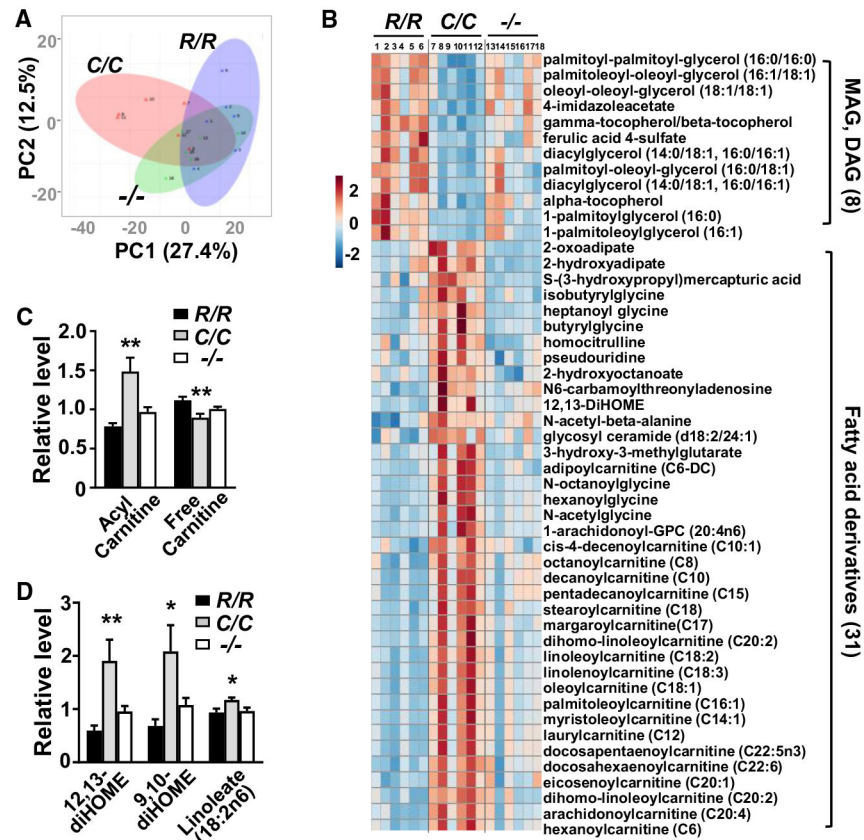


Figure 3. Plasma Metabolomic Profiling Reveals Altered Lipid Metabolism in *p53^{I78C/C}* Mice
 (A) Principal-component analysis (PCA) of all identified plasma metabolites of 10-week-old mice by *p53* genotype (n = 6).
 (B) Heatmap comparison of the top 50 most statistically different metabolites by *p53* genotype shows that 39 are lipid-related compounds. Metabolite levels were normalized by median values. Relative level is color-coded in red (increased) and blue (decreased). In *p53^{I78C/C}* (C/C) mouse plasma, 8 of the 12 decreased metabolites are monoacylglycerols (MAGs) and diacylglycerols (DAGs), and 31 of the 38 increased metabolites are fatty acid derivatives.
 (C) Relative levels of free carnitine and acyl carnitines (average of 32 different species).
 (D) Relative levels of 12,13-diHOME and its isomer 9,10-diHOME and precursor linoleate. *p53* R178 genotypes: wild-type (R/R), homozygous mutant (C/C), and null (-/-). Statistical difference by one-way ANOVA. Values are mean ± SEM. *p < 0.05, **p < 0.01. See also Figure S5.

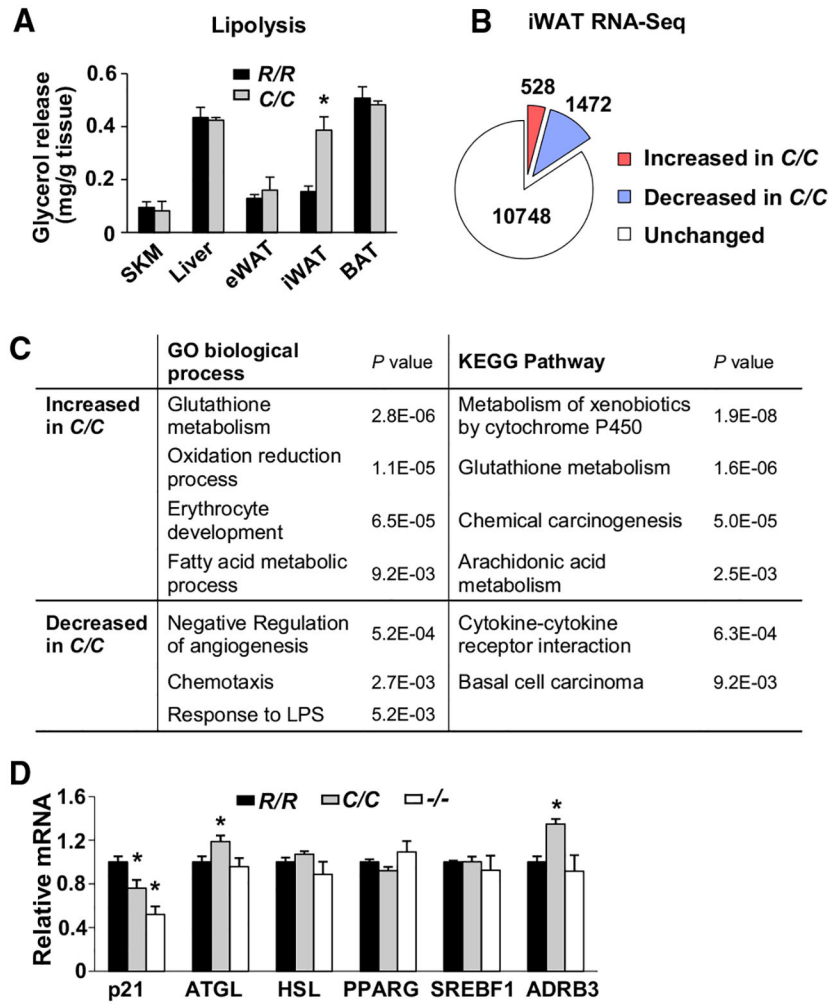


Figure 4. Increased Lipolysis and Expression of Genes Related to Fatty Acid Metabolism in iWAT of *p53^{178C/C}* Mice

(A) Release of glycerol into culture medium as a measure of basal lipolysis in the indicated tissue explants: skeletal muscle (SKM), liver, eWAT, iWAT, and BAT (n = 3).

(B) Number of genes identified by RNA-seq with significant changes in expression ($p < 0.05$) in the iWAT of *p53^{178C/C}* compared with *p53^{178R/R}* mice (n = 4).

(C) Gene Ontology (GO) and Kyoto Encyclopedia of Genes and Genomes (KEGG) pathway analysis of genes with significant expression changes in iWAT (>1.2 -fold or <0.8 -fold, $p < 0.05$).

(D) Relative expression levels of *p21* and some lipid metabolism genes in iWAT by *p53* genotype.

p53^{R178} genotypes: wild-type (*R/R*), homozygous mutant (*C/C*), and null (*-/-*). Statistical difference by two-tailed unpaired t test (A) and one-way ANOVA in comparison with the wild-type (*R/R*) (D). Values are mean \pm SEM. * $p < 0.05$. See also Figure S6.

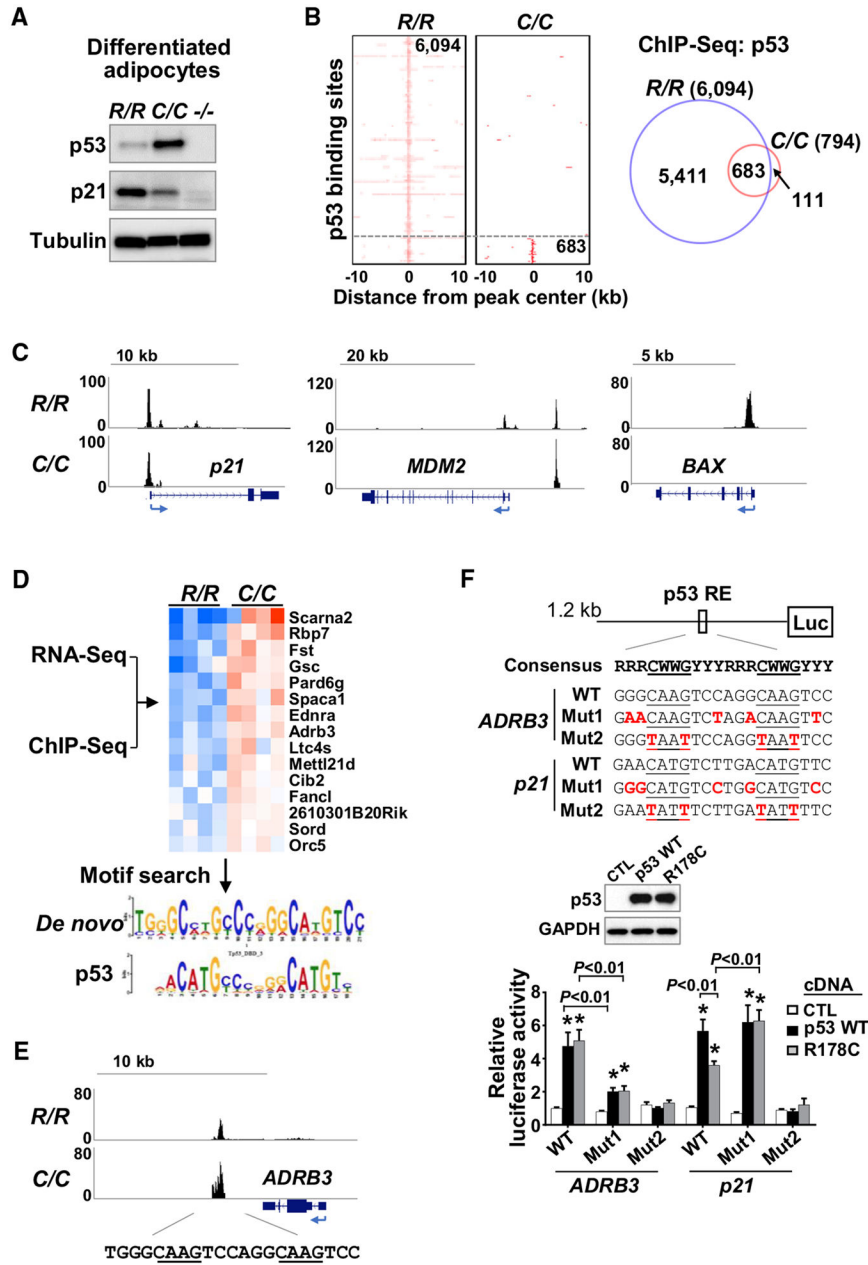


Figure 5. Identification of *ADRB3* as a Target Gene of p53 R178C Using ChIP-seq Analysis
 (A) Stromal vascular fractions (SVFs) isolated from iWAT of the indicated *p53* genotype mice, differentiated into adipocytes and analyzed by immunoblotting.
 (B) Heatmaps and Venn diagram of high-confidence (FDR < 1E-10) p53 binding sites from ChIP-seq analysis of *R/R* and *C/C* differentiated adipocytes described in (A).
 (C) Genome browser view of p53 binding peaks on known wild-type p53 target genes.
 (D) RNA-seq and ChIP-seq data were integrated to identify genes that are upregulated and bound by p53 R178C. p53-bound genomic sequences were subjected to a transcription factor motif search, which yielded a *de novo* motif (E value = 2E-44) matching the p53 binding motif (E value = 3E-5).
 (E) Genome browser view of *ADRB3* gene with the motif TGGGCAAGTCCAGGCAAGTCC.
 (F) Luciferase reporter assay for *ADRB3* and *p21* promoters. Relative luciferase activity is shown for CTL, p53 WT, and R178C genotypes. Significant differences are indicated by asterisks (*, **).

(E) ChIP-seq profile of the *ADRB3* gene region with sequences containing the consensus p53 RE.

(F) Effect of GC-rich sequences in the p53 RE of *ADRB3* on transactivation by p53, assessed by luciferase reporter assay. The GC-rich flanking sequences were mutated from GC to AT (Mut 1), and the p53 RE core sequence was also mutated as an additional negative control (Mut 2). The luciferase reporter constructs were co-transfected with wild-type p53, p53 R178C, or a control pcDNA empty vector (CTL) into *p53*^{-/-} 3T3L1 cells. p53 expression levels were assessed by immunoblotting (center panel), and luciferase activity levels of the respective constructs were measured (n = 4).

p53 R178 genotypes: wild-type (*R/R*), homozygous mutant (*C/C*), and null (*-/-*). Statistical difference by two-tailed unpaired t test in comparison with the vector control. Values are mean ± SEM. *p < 0.05. See also Table S1.

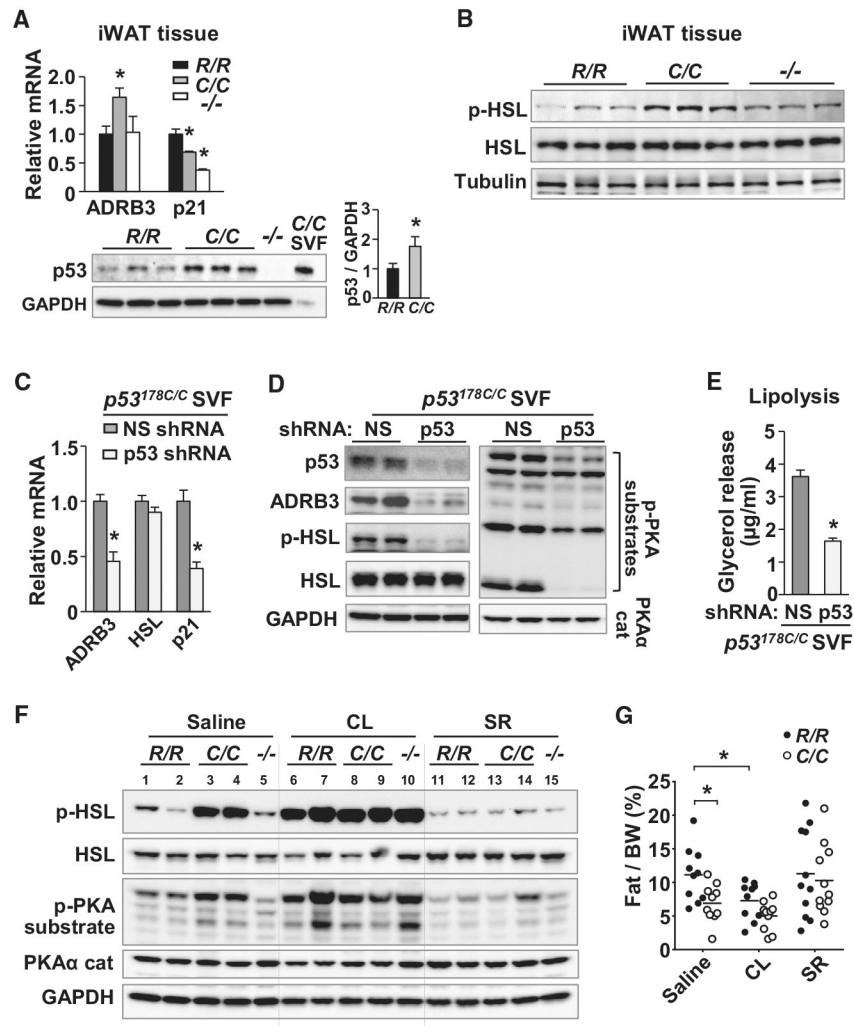


Figure 6. p53 R178C Promotes Lipolysis via ADRB3 Signaling

(A) *ADRB3* and *p21* mRNA levels measured by RT-PCR (top) and p53 protein expression evaluated by immunoblotting in iWAT of the indicated p53 genotype (n = 4). Adipocytes differentiated from *p53^{R178C/C}* SVF cells are shown as a positive control. p53 protein levels were quantified relative to GAPDH by densitometric scanning.

(B) Immunoblots of total and phosphorylated HSL (Ser-660, p-HSL) in iWAT (n = 3).

(C) SVFs isolated from iWAT of *p53^{R178C/C}* mice were transduced with a non-specific (NS) or p53 shRNA lentivirus, differentiated into adipocytes, and analyzed by RT-PCR (n = 3).

(D) The *C/C* adipocytes described in (C) were immunoblotted with antibodies, including those against phospho-PKA substrates (RRXS/T motif) and the PKA α catalytic subunit. Shown is one representative of 4 experiments with 3 biological replicates.

(E) Glycerol release into culture medium by *C/C* adipocytes transduced with shRNA as an *in vitro* measure of lipolysis activity (n = 4).

(F) Immunoblot of iWAT samples from the indicated p53 genotype mice after control saline, ADRB3 agonist CL316243 (CL), or ADRB3 antagonist SR59230A (SR) injection.

(G) Effect of daily injections of control saline, CL, or SR for 5 days on body fat composition of mice (~15 weeks old), measured by NMR analyzer (n = 10–11).

*p53*R178 genotypes: wild-type (*R/R*), homozygous mutant (*C/C*), and null (*-/-*). Statistical difference by one-way ANOVA (A) and two-tailed unpaired t test (B, E, and G). Values are mean \pm SEM. * $p < 0.05$. See also Figure S6.

Author Manuscript

Author Manuscript

Author Manuscript

Author Manuscript

KEY RESOURCE TABLE

REAGENT or RESOURCE	SOURCE	IDENTIFIER
Antibodies		
ADRB3	Thermo Fisher Scientific	Cat# PA5-50914; RRID:AB_2636362
α -Tubulin	Sigma-Aldrich	Cat# T5168; RRID:AB_477579
CD3e	eBioscience	Cat# 16-0031-86; RRID:AB_468849
CD28	eBioscience	Cat# 16-0281-86; RRID:AB_468923
GAPDH	Thermo Fisher Scientific	Cat# AM4300; RRID:AB_2536381
HSL	Cell Signaling Technology	Cat# 4107; RRID:AB_2296900
phospho-HSL (Ser660)	Cell Signaling Technology	Cat# 4126; RRID:AB_490997
phospho-PKA substrate (RRXS*/T*)	Cell Signaling Technology	Cat# 9624; RRID:AB_331817
PKA α cat (A-2)	Santa Cruz Biotechnology	Cat# sc-28315; RRID:AB_628136
p53 (1C12)	Cell Signaling Technology	Cat# 2524; RRID:AB_331743
p53 (FL393)	Santa Cruz Biotechnology	Cat# sc-6243; RRID:AB_653753
p21 (CDKN1A)	Millipore Sigma	Cat# OP76
TFAM	Abcam	Cat# ab131607; RRID:AB_11154693
Total OXPHOS Rodent Antibody Cocktail	Abcam	Cat# ab110413; RRID:AB_2629281
UCP1	Abcam	Cat# ab10983; RRID:AB_2629281
Control rabbit IgG	Santa Cruz Biotechnology	Cat# sc-2027; RRID: AB_737197
Chemicals, Peptides, and Recombinant Proteins		
CL316243	Sigma-Aldrich	Cat# C5976
Dexamethasone	Sigma-Aldrich	Cat# D1881
Dynabeads Protein A	Thermo Fisher Scientific	Cat# 10001D
Dynabeads Protein G	Thermo Fisher Scientific	Cat# 10007D
Indomethacin	Sigma-Aldrich	Cat# I7378
Insulin	Sigma-Aldrich	Cat# I5500
Isobutylmethylxanthine	Sigma-Aldrich	Cat# I7018
Oil Red O stain	American MasterTech	Cat# STORO100
SR59230A	Sigma-Aldrich	Cat# S8688
T3	Sigma-Aldrich	Cat# T2877
Ultrahyb solution	Ambion	N/A
Critical Commercial Assays		
Free Glycerol Reagent	Sigma	Cat# F6428
NEFA kit	Wako	Cat# 995-34791
RNeasy kit	Qiagen	Cat# 74104
Dual -Luciferase Reporter Assay System	Promega	Cat# E1960
QuikChange II Site-Directed Mutagenesis Kit	Agilent	Cat# 200523
In-Fusion HD Cloning Plus	Takara	Cat# 638920
NEBNext Ultra II DNA Library Prep Kit for Illumina	New England Biolabs	Cat# E7645
Senescence β -Galactosidase Staining Kit	Cell Signaling Technology	Cat# 9860
Deposited Data		
RNA-Seq	This paper	GSE132715

REAGENT or RESOURCE	SOURCE	IDENTIFIER
p53 ChIP-Seq Experimental Models: Cell Lines	This paper	GSE132715
3T3-L1 3T3-L1 <i>p53</i> ^{-/-} Experimental Models: Organisms/Strains	ATCC This paper	ATCC CL-173 N/A
Mouse: C57BL6/J Mouse: B6.129S2-Trp53tm1Tyj/J Mouse: C57BL6J < i > <i>Trp53</i> -R178C KI Oligonucleotides	Jackson Laboratory Jackson Laboratory This paper	JAX 000664 JAX 002101 N/A
See Table S2 Recombinant DNA	This paper	N/A
Mouse <i>p53</i> shRNA lentiviral plamid Lentiviral Packaging Mix pcDNA- <i>p53</i> R178C pLex- <i>p53</i> R178C Mouse <i>p53</i> CRISPR/Cas9 KO plasmid Software and Algorithms	OpenBiosystems Sigma-Aldrich This paper This paper Santa Cruz Biotechnology	TRCN0000012361 SHP001 N/A N/A Cat# sc-423059
GraphPad Prism 7.0 MetaboAnalyst 3.0 MEME/TOMTOM DAVID Bioinformatics Resources SICER SeqPos motif tool R Other	GraphPad Software MetaboAnalyst MEME Suite National Institutes of Health https://home.gwu.edu/~wpeng/Software.htm Galaxy Cistrome https://www.r-project.org/	N/A N/A N/A N/A N/A N/A N/A
Comprehensive Laboratory Animal Monitoring System (CLAMS) Minispec NMR analyzer	Columbus Instruments Bruker	N/A N/A